Hybrid Analog-Digital Backscatter: A New Approach for Battery-Free Sensing

Vamsi Talla and Joshua R. Smith
Department of Electrical Engineering
Department of Computer Science Engineering
University of Washington
Seattle, WA 98195
Email: vamsit@u.washington.edu and jrs@cs.washington.edu

***Abstract*— After comparing the properties of analog backscatter and digital backscatter, we propose that a combination of the two can provide a solution for high data rate battery free wireless sensing that is superior to either approach on its own. We present a hybrid analog-digital backscatter platform that uses digital backscatter for addressability and control but switches into analog backscatter mode for high data rate transmission of sensor data.**

Using hybrid backscatter, we report the first digitally addressable real-time battery free wireless microphone. We develop the hybrid backscatter platform by integrating an electret microphone and RF switch with a digital RFID platform (WISP). The hybrid WISP operates by default in digital mode, transmitting and receiving digital data using the EPC Gen 2 RFID protocol but switching into analog mode to backscatter audio sensor data when activated by Gen 2 READ command. The data is recovered using a USRP-based Software Defined RFID reader. We report an operating range of 7.4 meters for the analog backscatter microphone and 2.7 meters for hybrid microphone with 26.7 dBm output power USRP-based RFID reader.

I. Introduction

Radio Frequency Identification (RFID) systems have gained widespread acceptance for identification and tracking applications in supply chain management and building/transit access systems. The RFID industry has led this effort by developing long range and inexpensive tags, standardized protocols (EPC Gen2) and RFID reader infrastructure. Due to the tremendous progress made in this field, the sensing community has started exploring RFID technology to develop wireless sensing platforms and solutions [1]. Traditional approaches to sensing use battery powered devices which are bulky, expensive, short lived and need frequent battery maintenance. On the other hand, passive RFID tags harvest power from the electromagnetic waves transmitted by the reader and use backscatter to send information to the reader. Due to their small form factor and battery free operation, passive RFID sensors have longer lifetime and can be widely distributed and embedded virtually everywhere.

A. Digital backscatter sensing

Digital backscatter follows the conventional approach of sampling sensor data using an analog-to-digital converter (ADC) and transmitting sensor values as digital packets to the reader. A digital temperature sensor using a custom integrated circuit operating in UHF frequency band has been reported in literature [2]. An alternative approach to custom IC, is the use of programmable platforms such as the Wireless Identification and Sensing Platform (WISP) which enable flexibility in the choice of sensing applications. Using WISP, a multitude of sensing applications such as accelerometer, light sensor, temperature sensor and strain gauge have been reported [3]. Although digital backscatter provides noise immunity and enables the use of existing protocols (and features such as addressability and control) and RFID reader infrastructure, the typical power requirements of active sensors and ADCs are higher than what is available from the reader at long distances. This results in limited operating range and/or low duty cycles for the digital backscatter platform. Lastly, existing protocols (such as EPC Gen2) are optimized for identification and do not support high data rate streaming of sensor data [1].

B. Analog backscatter sensing

Analog backscatter is an alternative sensing approach where the sensing quantity (e.g. temperature) directly modifies some characteristics (such as quality factor or resonant frequency) of a resonating structure or an antenna. For example, Theremin's cavity resonator (also known as the Great Seal Bug [4]) uses capacitive changes in a flexible metallic membrane to detect sound waves. In [5] electromagnetic and magnetomechanical resonance is to develop position and force sensors. Recent work in RFID sensing has focused on utilizing the antenna of commercial RFID tags as a sensor. RFID tag antennas coated with a sensing film or when brought in proximity of metals/dielectric result in change in the read rate, operating range and turn-on power of the tag. These changes can be detected to develop humidity sensors [6], displacements sensors, and temperature sensors [7]. However, tag antenna based sensing has very limited resolution and is limited to slowly varying quantities. Furthermore, a common drawback in tag based antenna sensing is the need for continuous calibration of the RF channel to mitigate path loss and multipath effects.

C. Hybrid backscatter sensing: This work

Traditional analog backscatter requires specialized antennas/resonant structures which are incompatible with standard digital backscatter. In this work, we implement analog

978-1-4673-5750-0/13/$31.00 ©2013 IEEE

backscatter by directly connecting the antenna to a sensor whose impedance varies as a function of the sensed quantity. Using this approach of analog backscatter, we undertake a comparative study of analog *vs.* digital backscatter. We conclude that the optimal solution for high data rate sensing is a hybrid platform that combines addressable digital backscatter with selectable sensors which use analog backscatter for high data rate sensing. We demonstrate our approach of hybrid backscatter by augmenting a digital RFID platform (WISP) with a microphone to develop the first digitally addressable battery free microphone.

We previously introduced the hybrid approach and presented preliminary results in [8]. In this paper, we undertake a comparative study of analog *vs.* digital backscatter to motivate the use of hybrid backscatter platforms. We also conduct an in-depth analysis of the working of the backscatter microphone. Based on this analysis, we optimize the backscatter microphone design and report substantial improvements in performance (compared to [8]). The outline of the paper is as follows. In Section II we discuss the basics of backscatter communication followed by a comparative study of analog and digital backscatter sensing in Section III and hybrid backscatter in Section IV. In Section V we discuss a backscatter microphone and our implementation of hybrid backscatter platform is discussed in Section VI. Experimental setup and results of the hybrid backscatter platform equipped are presented in Section VII and Section VIII concludes the paper with remarks on future work.

II. Theory

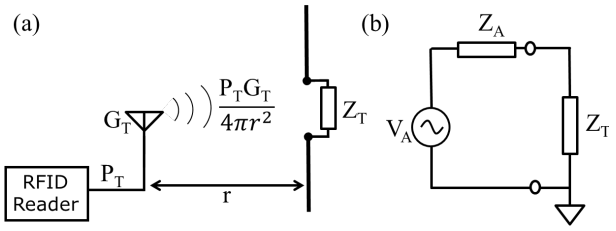

Fig. 1. (a) A typical RFID system (b) Equivalent model of antenna

Figure 1(a) illustrates a typical RFID system which consists of an RFID reader transmitting electromagnetic waves with RFID tag(s) located in its vicinity. The power density of electromagnetic waves incident on a tag placed at a distance r from the reader is given as

$$S = \frac{P_t G_t}{4\pi r^2} \tag{1}$$

where P_t is the power transmitted by the reader and G_t is the gain of the reader antenna.

The incident power is collected by the aperture of the tag antenna and delivered to the terminating impedance. Simultaneously, a fraction of the incident power is scattered by the antenna. The analysis in this work of received and backscattered power is based on the Thevenin equivalent circuit model shown in Figure 1(b) where V_A is the open circuit voltage on the antenna terminals, $Z_A = R_A + jX_A$ is the complex antenna impedance and $Z_T = R_T + jX_T$ is the impedance across the antenna terminals [9].

A. Power Harvesting and Duty Cycle Operation

The RF power collected by the tag is determined by the effective aperture of its antenna (A_e) and is given by

$$P_{received} = SA_e = \frac{P_t G_t}{4\pi r^2} . \frac{\lambda^2 G_r}{4\pi} \left[1 - |\Gamma|^2\right] \tag{2}$$

where, G_r is the gain of the receive antenna, λ is the wavelength and Γ, the reflection coefficient is defined as

$$\Gamma = \frac{Z_T - Z_A^*}{Z_A + Z_T} \tag{3}$$

For maximum power transfer ($|\Gamma| = 0$), the antenna should be terminated by the complex conjugate of its impedance i.e. $Z_T = Z_A^*$. This represents the matched impedance state which is optimal for power harvesting.

As seen from (2), the power received by the tag drops rapidly as the distance between the tag and the reader increases. Typical sensing platforms have significant power consumption and they operate by duty cycling their operation [3]. During the sleep/off state, the circuit continuously harvests energy while consuming minimal power. Once sufficient energy is available, the system wakes up and executes a task (sensing, computation and communication). By equating the energy harvested with the total energy consumed over each operating cycle and using (2), the duty cycle (D) of the system can be estimated as

$$\begin{aligned} D &= \frac{T_{on}}{T_{on} + T_{sleep}} = \frac{P_{received} * \eta_{harvester} - P_{leakage}}{P_{load}} \\ &= \frac{\frac{P_t G_t}{4\pi r^2} . \frac{\lambda^2 G_r}{4\pi} \left[1 - |\Gamma|^2\right] * \eta_{harvester} - P_{leakage}}{P_{load}} \end{aligned} \tag{4}$$

where $\eta_{harvester}$ is the efficiency of the power harvester, $P_{leakage}$ is leakage power consumption (during sleep/off mode) and P_{load} is the average power consumption of the active mode (excluding leakage power). It can be seen that the maximum operating range of the system is the distance at which the harvested power is equal to leakage power and the duty cycle drops to zero. Note that the maximum operating range is a function of leakage power and is independent of active power consumption.

B. Backscatter Communication

Passive RFID tags modulate the impedance across the antenna terminals which causes a change in the field backscattered by the tag. These changes in the field are detected by the reader and are used to decode the bits transmitted by the tags. For thin wire antennas such as dipoles which are used in RFID tags, the re-radiated can be computed using the equivalent circuit model [9] shown in Figure 1(b) and can be written as

$$P_{backscatter} = S\sigma = \frac{P_t G_t}{4\pi r^2} . \frac{\lambda^2 G_r^2}{4\pi} |1 - \Gamma|^2 \tag{5}$$

where, σ, the scalar radar cross section (RCS) of the antenna is defined as

$$\sigma = \frac{\lambda^2 G_r^2}{4\pi} |1 - \Gamma|^2 \quad (6)$$

The backscattered field from the tag antenna undergoes path loss in the reverse direction and the signal power received by the reader located at a distance r from the tag is given as

$$P_{reader} = \frac{P_{backscatter} A_e}{4\pi r^2} = \frac{P_t G_t^2 \lambda^2 \sigma}{(4\pi)^3 r^4} \quad (7)$$

where σ is defined in (6). Subsequent analysis of backscatter communication will consider that all antennas are operating at their resonant frequency i.e. the frequency at which $Z_A = R_A$.

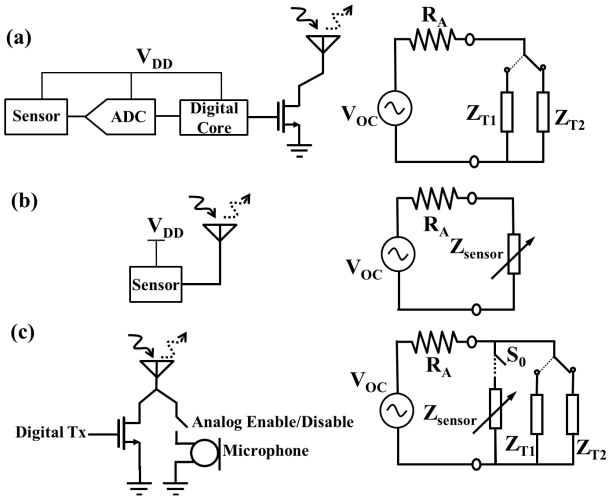

Fig. 2. (a) Digital backscatter sensing platform (b) Analog backscatter sensing platform (c) Hybrid analog-digital backscatter sensing platform

1) Digital Backscatter Sensing: A typical digital backscatter sensing platform (shown in Figure 2(a)) uses an ADC to sample the output of the sensor. The digitized sensor data is then processed and transmitted as binary data packets by using a FET to switch the impedance across the antenna between matched ($Z_{T1} = R_A$) and short ($Z_{T2} = 0$) states. This switching operation implements binary amplitude/phase shift keying and maximizes the difference in the power backscattered by the tag (while being able to simultaneously harvest in one state). The difference in the backscattered digital power received by the RFID reader is typically analyzed using differential radar cross section [10], and in the ideal case of switching between matched and short states can be written as

$$P_{reader\_d} = \frac{P_t G_t^2 \lambda^2 \Delta\sigma}{(4\pi)^3 r^4} = P_t G_t^2 G_r^2 \left(\frac{\lambda}{4\pi r}\right)^4 \quad (8)$$

2) Analog Backscatter Sensing: Analog backscatter generalizes the concept of backscatter by continuously varying the terminating impedance of the antenna. Traditional approaches to analog backscatter use the antenna as the sensing element [6], [7]. However, our approach to analog backscatter sensing (as shown in Figure 2(b)) consists of a sensor (passive or active) directly connected to the terminals of the antennas. The impedance of the sensor (Z_{sensor}) varies as a function of the sensing quantity, thereby, modulating the backscatter power with sensor information. Using (3), (6) and (7), the analog backscattered power as a function of the impedance of the sensor can be written as

$$P_{reader\_a} = \frac{\lambda^4 P_t G_t^2 G_r^2}{(4\pi r)^4} \frac{4R_A^2}{|R_A + Z_{sensor}|^2} = f(Z_{sensor}) \quad (9)$$

The reader captures the backscattered power and uses (9) to decode, digitize and process the sensor information. Under certain conditions (as shown in Section V) the decoding process can be as simple as a band pass filter.

3) Hybrid Analog-Backscatter Sensing: Analog and digital backscatter can be combined to develop a hybrid backscattering platform. Figure 2(c) shows a schematic and equivalent circuit model for a hybrid backscattering platform which time multiplexes digital and analog backscatter modes. In the digital backscatter mode, the analog switch (S_0) is turned off, disconnecting the sensor from the antenna, and the platform behaves as a normal digital backscatter platform as described in Section II-B.1. In analog backscatter mode, the analog switch (S_0) is turned on, connecting the sensor (in parallel with the terminating impedance, Z_{T1}) to the antenna. The backscattered power as a function of the impedance of the microphone (Z_{sensor}) sensor can be written as

$$P_{reader\_h} = \frac{\lambda^4 P_t G_t^2 G_r^2}{(4\pi r)^4} \frac{4R_A^2}{|R_A + Z_{T1} \,||\, Z_{sensor}|^2} \quad (10)$$

III. Analog Backscatter versus Digital Backscatter

A comparative study of analog $vs.$ digital computation has been reported in literature which shows that for a given bandwidth (set by the specifications of the task), analog performs better (in terms of both chip area and power) for low signal to noise ratios whereas digital has better performance for high signal to noise applications [11]. It was concluded that for any given task, the optimal solution was neither analog nor digital alone, but a combination/hybrid of both analog and digital computation. In this section, we undertake a similar ***qualitative*** study to understand the performance of analog backscatter sensing and digital backscatter sensing in terms of power consumption, duty cycle and signal to noise ratio.

A. Power Consumption

The power consumption ($P_{digital}$) of a digital backscatter platform (in Figure 2(a)) consisting of an active sensor (including amplifiers and anti-aliasing filters), ADC, digital core and the switching transistor can be written as

$$\begin{aligned} P_{digital} &= P_{sensor} + P_{core} + P_{ADC} \\ &= P_{DC} + CV_{DD}^2 f_s + FOM * 2^{ENOB} * f_s \end{aligned} \quad (11)$$

where, P_{DC} is the static power consumption of the sensor (and associated amplifiers and anti-aliasing filters). C represents the effective capacitance switching at sampling frequency (f_s) in the digital core and FET. *FOM* is the figure of merit of

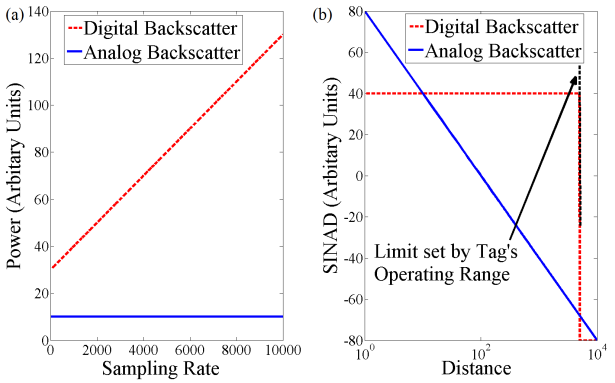

Fig. 3. (a) Tradeoff between power consumption and sampling rate (b) Tradeoff between *SINAD* and distance

the ADC and *ENOB* represents the ADC's effective number of bits [12].

A typical analog backscatter sensing platform (Figure 2(b)) consists of a passive sensor (such as thermistors, light dependent resistor, microphone) directly connected to the antenna. However, for completeness let us express the power consumption as

$$P_{analog} = P_{sensor} = P_{analog\_DC} \tag{12}$$

In analog backscatter, sampling and subsequent filtering of sensor data is done by the reader. This enables the sensor data to be sampled and filtered/processed at high rates independent of the power constraints of the sensing platform. Hence, the power consumption of an analog backscatter platform is independent of sampling frequency.

Figure 3(a) shows a comparison of the power consumption in terms of sampling rate. The power consumption of the digital system increases linearly with increasing sampling frequency whereas the power consumption of the analog system is constant. Hence, analog backscatter is a more power efficient technique for sensing. Please note the preceding analysis does not take into account the loss in the harvested power during backscatter communication.

B. Signal to Noise and Distortion Ratio (SINAD)

In typical digital backscatter systems, as long as the tag is within the operating range of the reader, the digital communication from the tag to the reader can be considered error free. In such a scenario, the noise is limited by the ADC front end and the signal to noise and distortion ratio (*SINAD*) of digital sensor data is a function of *ENOB* and can be written as [12]

$$SINAD_{digital} = ENOB * 6.02 + 1.76dB \tag{13}$$

For analog backscatter systems, the sensor information is modulated with the backscattered power. Using (7), *SINAD* of sensor data as a function of distance between the reader and the tag can be written as

$$SINAD_{analog} = 10 * log_{10}\left(\frac{P_0}{r^4\left(P_d + N\right)}\right) \tag{14}$$

where, P_0 is the backscatter power received at unit separation, P_d is the distortion and N is the noise floor of the RF front end of the reader.

Figure 3(b) shows a comparison of *SINAD* between analog and digital backscatter systems across a range of operating distances. It can be seen that *SINAD* of analog backscatter drops at the rate of 40 dB/decade with increase in distance (equivalently 10 dB/decade drop with path loss) whereas digital backscatter has a near constant value till the maximum operating range. So, for applications which require high signal to noise ratio, digital backscatter is better suited (assuming there is no power constraint).

C. Duty Cycle

As shown in Section II-A, the high power consumption of digital backscatter systems requires that RF powered digital backscatter systems be duty cycled. Using (4), the duty cycle of digital backscatter systems can be expressed as

$$\begin{aligned} D_{digital} &= \frac{P_{DC\_received}}{r^2 P_{digital}} \\ &= \frac{P_{DC\_received}}{r^2\left(P_{DC} + CV_{DD}^2 f_s + FOM * 2^{ENOB} * f_s\right)} \end{aligned} \tag{15}$$

where, $P_{DC\_received}$ is available DC power from the harvester at unit distance. As sampling frequency increases the power consumption of digital systems increases, which forces a reduction in the duty cycle of digital systems. Similarly, the power available from the reader reduces with increase in distance, which results in reduction of duty cycle for the digital backscatter system.

On the other hand, typical analog backscatter systems are passive, consuming zero/minuscule power. For the distances under consideration, analog backscatter systems are always active or in other words they operate at 100% duty cycle. Hence, for applications which require high duty cycles (response rate), analog backscatter is better suited (neglecting *SINAD* of sensor data).

D. SINAD for reconfigurable ADCs

Typical digital backscatter systems have ADCs with fixed resolution (*ENOB*) which determines the *SINAD* of digital sensor data. This has been the premise in previous sections. Here we will consider the scenario where the resolution of the ADC can be modified. This could be accomplished in the design phase of the ADC, or in the case of reconfigurable ADC's, the digital core can modify the resolution (and hence the power consumption) on the fly. This enables us to study the maximum achievable *SINAD* for digital backscatter as a function of sampling frequency and distance. (15) can be rearranged and the *ENOB* of the ADC can be written as

$$\begin{aligned} ENOB = log_2\left(\frac{P_{DC\_received}}{r^2 D} - P_{DC} - CV_{DD}^2 f_s\right) \\ - log_2\left(f_s FOM\right) \end{aligned} \tag{16}$$

Using (13) and (16), *SINAD* of digital backscatter system can be ascertained. Note that *ENOB* is a function of three parameters (r, f_s and D) which complicates the analysis. Since duty cycle was analyzed above, we will assume a fixed duty cycle digital backscatter system for this analysis.

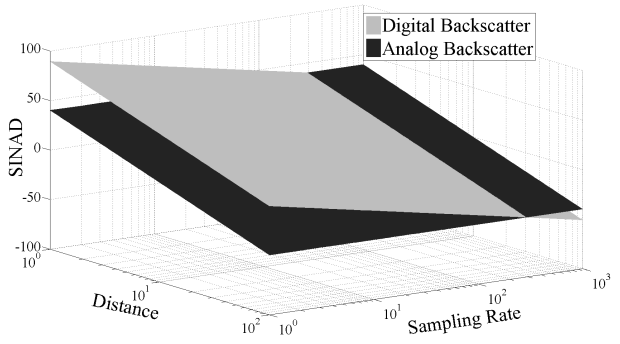

Fig. 4. Study of tradeoff between *SINAD*, distance and sampling rate for analog and digital backscatter sensing

For analog backscatter system, (14) can be used to determine *SINAD* as the function of distance and sampling rate. Figure 4 plots the variation of *SINAD* of analog and fixed duty cycle digital backscatter systems with distance and sampling frequency. As discussed above, *SINAD* of analog backscatter is independent of sampling rate but drops with increasing distance. For digital backscatter systems, since power received from the reader decreases with increases in distance, *SINAD* has to be decreased to reduce power consumption. Similarly, as sampling frequency increases, the power consumption of digital backscatter increases which has to be compensated with a reduction of *SINAD*. Hence, in terms of *SINAD*, digital backscatter performs better at low sampling rates whereas analog backscatter is preferred for high sampling rates.

In conclusion it can be seen that digital backscatter is better suited for low sampling rate and/or low response rate sensing applications, whereas, analog backscatter is better suitable for high sampling rate applications. Note that the above analysis is generic and device independent and has been performed to understand the inherent tradeoffs and trends in analog and digital backscatter sensing. The actual regions of tradeoff depend on the characteristics of the sensor employed and the specific requirements of the sensing application.

However, it should be acknowledged that as technology scales, digital computation becomes more power efficient [13]. This implies that digital backscatter sensing platforms will be able to operate at higher sampling rates, at higher duty cycles and at farther distances from the reader. Unfortunately, analog sensors and analog backscatter do not follow the same trend. Additionally, new digital signal processing techniques such as compressing sensing could potentially enable digital platforms to accomplish the sensing goal at lower sampling rates. Hence, trends in semiconductor technology and signal processing favor digital backscatter for sensing applications.

IV. Hybrid Sensing

In addition to the quality (*SINAD*) of sensor data, typical applications require multiple sensors (with a wide range of sensor data quality and sampling rate specifications), addressability, selectivity and control. Unfortunately, all the requirements cannot be satisfied by either analog or digital backscatter independently. The optimal solution is to use digital backscatter for addressability, control and low sampling/update rate sensing and analog backscatter (addressed and controlled digitally) for high data rate sensing. This can be accomplished by combining analog and digital backscatter into a hybrid backscatter platform. Another advantage of hybrid sensing is that hybrid backscatter utilizes the same quasi-static RF channel (for typical switching periods) for digital and analog backscatter communication. Since digital backscatter switches between two pre-determined states, it can be used to estimate the characteristics of the channel and in turn calibrate analog backscattered signal/sensor data.

V. Real Time Battery Free Microphone

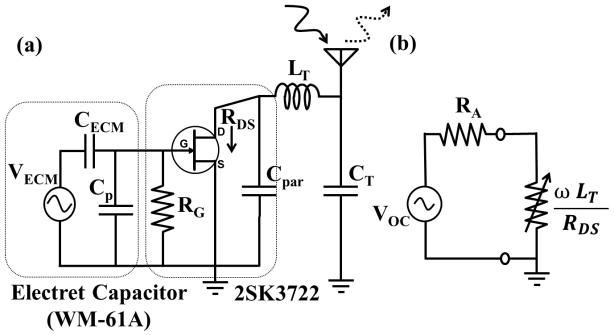

Fig. 5. (a) Equivalent model of the WA61A microphone connected to antenna to transmit audio data using analog backscatter (b) Equivalent model for analog backscatter analysis

Audio/speech is a very popular sensed quantity which finds numerous applications in human smart spaces. Battery free wireless detection of heart sounds (250 Hz bandwidth) has been reported in [14]. However, wireless transmission of audio and speech on RF powered systems has been a challenge due to the sampling rate ($\geq$ 6.8 kHz) requirements. These are relatively high rates for backscatter sensing. Typical applications (such as speech recognition) require a minimum time duration (typically 75 ms or more) of continuously sampled data for processing. This implies that each operating cycle must capture, process, packetize and transmit 75 ms long samples. Such high cumulative power consumption severely cripples the duty cycle of the digital system. As an example, let us consider integrating an off the shelf low power digital microphone (*MP45DT02*) with the WISP. The active power consumption of WISP is 1.12 mW and *MP45DT02* has an additional power consumption of 1.17 mW (650 μA at 1.8V). At a nominal distance of 2 m from the reader, ignoring protocol limitations, the maximum achievable duty cycle for the system is 7.8% i.e. the WISP can transmit one cluster

of samples (75 ms long) every second. Moreover, this rate rapidly drops with each increase in distance. Such low and varying data rates are impractical for current implementations of typical applications (such as speech recognition and event detection). Although the use of WISP and *MP45DT02* is not the optimal approach, it illustrates the limitations of digital backscatter platforms in transmission of speech.

Analog backscatter systems can transmit continuously at high data rates in real time. Furthermore, human ears and speech recognition software are capable of processing noisy speech data. Taking these factors into account, analog backscatter which can accommodate high data rates (at near zero power), albeit at distance-dependent SNR, is a good candidate for transmission of speech on RF powered platforms.

To demonstrate analog backscatter of audio/speech, we chose an electret condenser microphone (*WM61A* by Panasonic). Electret condenser microphones (ECM) use electret material (which has a quasi-permanent electrostatic charge) as the microphone's diaphragm. The electret diaphragm is separated from a fixed metal back plate by an air gap, forming a capacitor. As sound waves move the diaphragm, the distance between the electret diaphragm and the metal back place changes, resulting in a change in the capacitance. Since the charge stored on the electret diaphragm is fixed, this results in small signal voltage change. Thus, the electret capacitor can be simply modeled as a capacitive voltage source (V_{ECM}) in series with a $2 \sim 5pF$ capacitor (C_{ECM}) as shown in Figure 5(a). Because the output impedance of the electret capacitor is very high, a high input-impedance (modeled as R_B) device such as a JFET ($2SK3722$) is connected to its output.

Let P_{audio} be the pressure of the audio waves striking the diaphragm. The voltage induced at the drain source terminal can be written as

$$V_{GS} = k_{ECM} * P_{audio} \tag{17}$$

where k_{ECM} accounts for the transducer gain of the electret diaphragm and the voltage transfer from V_{ECE} to V_{GS}. In traditional applications, the JFET is biased in saturation region using an external DC bias and a load resistor to operate as a common source amplifier. However, to implement analog backscatter, we directly connect the source terminal of the JFET to the antenna (using an L-C tuning network) as shown in Figure 5. Since there is no DC voltage on the drain terminal, the voltage across the drain and source terminals of the JFET, $V_{DS} \approx 0$, biasing the device in the triode region. In triode region, the impedance looking into the drain terminal of the JFET can be written as

$$R_{DS} = \frac{R_{DS\_ON}}{\left(1 - \frac{V_{GS}}{V_p}\right)} \tag{18}$$

where, V_p is the pinch-off voltage and R_{DS_ON} is the impedance looking into the drain terminal for $V_{GS} = 0$. In order to tune the input impedance of the JFET to the impedance of the antenna, an L-C tuning network is employed and for typical values of quality factor (≥ 4), the impedance of the microphone as seen by the antenna can be written as

$$R_{sensor} = \frac{\omega^2 L_T^2}{R_{DS}} = R_s \left(1 - \frac{V_{GS}}{V_p}\right) \tag{19}$$

where, R_s is the impedance seen by the antenna for zero audio/speech input. The signal received by an RFID reader is typically analyzed in the voltage domain. Using the equivalent circuit model shown in Figure 5(b) and combining (19) and (9), the backscatter signal (in terms of scalar voltage) received at the reader can be written as

$$\begin{aligned} V_{reader\_a} &= \frac{K}{R_A + R_s\left(1 - \frac{V_{GS}}{V_p}\right)} \\ &\approx \frac{K}{R_A + R_s}\left[1 + \frac{V_{GS}}{V_p}\left(\frac{R_s}{R_A + R_s}\right)\right] \\ &= \frac{K}{R_A + R_s} + \frac{k_{ECM}}{V_p}\frac{KR_s}{\left(R_A + R_s\right)^2} P_{audio} \end{aligned} \tag{20}$$

where K incorporates the gain of the RF front end, path loss, transmit power and antenna parameters. For typical values of V_{GS} (10's of mV), the binomial approximation can be used to write the voltage as a linear function of the sound input (as shown in (20)). For maximum gain/sensitivity, $R_s = R_A$ i.e. the impedance of microphone for zero input should be matched to antenna impedance. Compared to the unoptimized system first reported in [8], this matching increases the sensitivity of the microphone by at least 15 dB.

Similarly, for a hybrid microphone using (19) and (10) wherein $Z_{T1} = R_A$ (for optimal power harvesting), the backscatter signal (in terms of scalar voltage) received at the reader can be written as

$$V_{reader\_h} = \frac{K\left(R_A + R_s\right)}{R_A\left(R_A + 2R_s\right)} + \frac{k_{ECM}}{V_p}\frac{KR_s}{\left(R_A + 2R_s\right)^2} P_{audio} \tag{21}$$

In case of a hybrid microphone, maximum sensitivity is achieved for $R_s = R_A/2$. Note that the hybrid microphone is less sensitive than pure analog backscatter microphone by a factor of 3 dB. However, given the additional benefits of hybrid backscatter, the loss in sensitivity is acceptable for typical sensing applications.

VI. Hybrid Analog-Digital Backscatter Sensing Platform

To demonstrate the concept of hybrid backscatter, we developed a hybrid analog-digital backscatter platform by leveraging the micro-controller based Wireless Sensing and Identification platform (WISP) [3]. WISP is an RF-powered platform featuring a fully programmable 16-bit micro-controller ($MSP430$) and an array of sensors, that communicates with commercial RFID readers at 915 MHz using the EPC global Class-1 Generation-2 (Gen 2) protocol. We integrated the backscatter microphone discussed in section V with the WISP to design a hybrid WISP. The hybrid WISP by default operates in digital mode and switches into analog mode to backscatter analog audio sensor data.

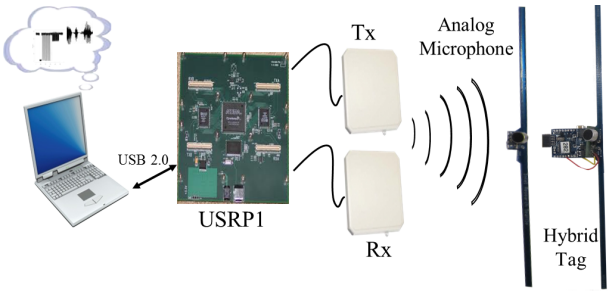

Fig. 6. Experimental Setup consists of a USRP based RFID reader and the backscatter microphones

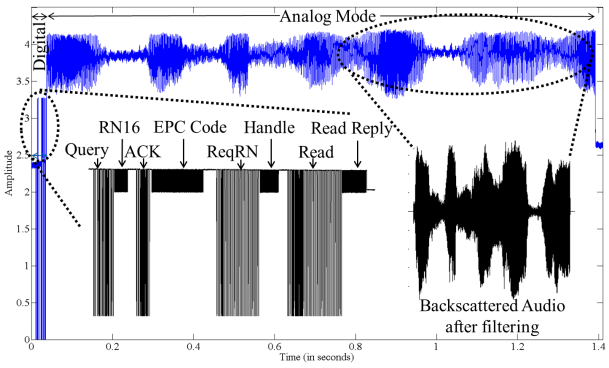

Fig. 7. The signal trace of a communication cycle between the hybrid WISP and the software defined RFID reader

A. Hybrid WISP Design

As shown in Figure 2(c), the RF front end of the hybrid WISP consists of a dipole antenna connected to the digital backscatter MOSFET (*BF1212WR*) in parallel to the microphone. The microphone is switched in and out of the backscatter network using an RF switch (*ADG902*). The RF switch and the digital backscatter MOSFET are both controlled by the output ports of the WISP micro-controller. WISP implements the Gen 2 protocol completely in firmware, and we modified its state-machine so that it transitions into analog backscatter mode when it receives a Gen 2 *READ* command that is addressed to it. After a configurable amount of time, the firmware switches the microphone out of the antenna network and returns to digital mode. During the analog mode, although the microphone consumes zero power, the MSP430 micro-controller operates in low power mode (LPM3) consuming 4.5 μW. This power consumption is miniscule and only fractionally more than the leakage power (2.9 μW) of WISP which enables the hybrid WISP to remain in analog mode for substantial period of time (e.g. few seconds for 100 μF storage capacitor).

B. Custom RFID Reader Design

To experimentally demonstrate our approach to hybrid backscatter, we extended a software-radio based Gen 2 reader previously developed using the Universal Software Radio Peripheral and GNU Radio [15]. The RFID reader and the hybrid WISPs by default operate in digital mode, where the reader continuously executes inventory rounds to query for WISPs that are present in the vicinity. During a query round, the reader can selectively transition a given WISP to analog mode by transmitting Gen 2 *READ* command addressed to that WISP. Once in analog mode, the hybrid WISP backscatters sensor (audio) data for a predetermined period of time and the RFID reader logs the digitized sensor data. At end of this time, the WISP transitions back to digital mode and the reader continues to query for other WISPs. The sensor (audio) data is recovered by passing the logged data through a band pass filter (300 Hz-3.4 kHz in case of speech) using GNU Radio signal processing blocks on the reader.

VII. Results and Discussion

Figure 7 shows a communication cycle between the hybrid WISP and the software defined RFID reader. The reader initiates a query round and receives the WISP ID as a part of the EPC code. The reader then issues a *READ* command upon which the hybrid WISP transitions into the analog mode, backscattering analog sensor (audio) data. The inset on the left shows the EPC Gen2 commands transmitted between the reader and the WISP. The right inset shows a magnified image of the recovered speech by the reader.

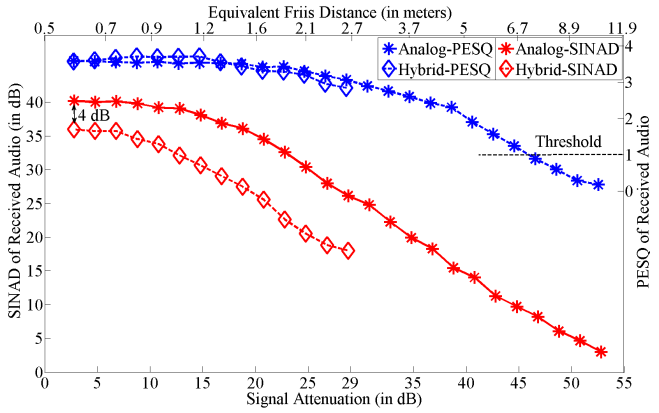

Fig. 8. Performance of analog backscatter and hybrid backscatter microphone

The experimental setup shown in Figure 6 was used to evaluate the performance of the backscatter microphone. The analog/hybrid microphone and the reader antennas were placed 0.5 m apart at a height of 1 m from the ground and the reader was configured to transmit at maximum power (26.7 dBm). To minimize multipath effects, path loss was introduced using variable attenuators in the forward and return path. A constant tone at mid band frequency (1.75 Khz at 90 decibels) and a reference audio clip (at 90 decibels) were played as input to the microphone to evaluate *SINAD* and Perceptual Evaluation of Sounds Quality (*PESQ*) scores [16] respectively.

Figure 8 shows the quality of speech received from the analog and hybrid microphone as a function of RF signal strength and Friis equivalent distance. The *SINAD* of received

speech decreases linearly (at rate of 10 dB/decade) with signal attenuation which agrees with our hypothesis. Analog backscatter microphone performs better than the hybrid backscatter microphone by a factor of 4 dB which is along expected lines. 3 dB difference was predicted in Section V and the additional 1 dB can be attributed to loss in the switch and impedance mismatch. However, for short distances (up to 1 m), the power received by the tag is very high, which introduces non-linearity in the JFET and results in saturation. Lastly, as path loss increases, hybrid backscatter starts to degrade at a rate higher than the predicted 10 dB/decade. This is most likely due to mismatches introduced by the non-linear variations in the input impedance of the harvester.

Since the quality of the received audio is a function of distance, the maximum operating range of the system is determined by the minimum acceptable *SINAD* and/or *PESQ* by the application. As an example, for human hearing, $PESQ \geq 1.0$ is decipherable and the expected operating range of analog microphone in this case is 7.4 m. The hybrid microphone works up to 2.7 m which is the maximum operating range of the WISP for 26.7 dBm reader output power. However, if the microphone is integrated with an RFID platform with larger operating range, extrapolating the graph, the expected operating range of the hybrid microphone would be 4.7 m.

Although the use of USRP as RFID reader provides flexibility, it has some limitations. The maximum transmit power of USRP is 26.7 dBm which is 3.3 dBm lower than the limit imposed by FCC (for 36 dBm EIRP). Increase in transmit power of the reader to 30 dBm would result in a 20% increase in the operating range of the analog backscatter microphone and 40% increase in the operating range of hybrid backscatter microphone. The RF front end of the USRP is not optimal and has higher noise floor than commercial RFID readers, which results in significant signal degradation. Use of a lower noise factor RF front end can substantially increase the *SINAD* of received audio and extend the operating range of the microphone.

VIII. Conclusion and Future Work

We have undertaken a comprehensive study of analog and digital backscatter sensing. After careful analysis, we concluded that the optimal strategy for high data rate battery free sensing is a hybrid of analog and digital backscatter sensing. This approach combines the addressability and control of digital backscatter with high data rate (and low/zero power) analog backscatter sensing. We have demonstrated a practical implementation of hybrid backscatter and developed an addressable real-time battery free microphone. The battery free hybrid microphone operates at a distance upto 2.7 m with a 26.7 dBm transmit power reader. Use of a 30 dBm output power reader should extend the operating range to 4.5 m (operating range of WISP). Such battery free microphones can be used to develop battery free voice communicators, audio event detectors and audio based localizers for pervasive computing applications.

In the future, we propose to study the observed non-linear effects of variations in harvester impedance and the saturation of the microphone JFET under high power conditions. We will investigate microphones with higher sensitivity and RFID readers with increased transmit power and lower noise floor RF front end to improve the quality of the received audio and extend the operating range. We also propose to explore alternate sensors such as thermistors and light dependent resistors which can used for analog backscatter sensing. Finally, we are working on the use of digital backscatter to calibrate the analog backscattered sensor data, which was briefly discussed.

IX. Acknowledgment

This work was funded by NSF (Grant No. EEC-1028725) and the Intel Science and Technology Center for Pervasive Computing (ISTC-PC).

References

[1] S. Roy, V. Jandhyala, J. Smith, D. Wetherall, B. Otis, R. Chakraborty, M. Buettner, D. Yeager, Y.-C. Ko, and A. Sample, "Rfid: From supply chains to sensor nets," *Proceedings of the IEEE*, vol. 98, no. 9, pp. 1583 –1592, sept. 2010.

[2] S. Park, C. Min, and S.-H. Cho, "A 95nw ring oscillator-based temperature sensor for rfid tags in 0.13 um cmos," in *Circuits and Systems, 2009. ISCAS 2009. IEEE International Symposium on*, may 2009, pp. 1153 –1156.

[3] A. Sample, D. Yeager, P. Powledge, A. Mamishev, and J. Smith, "Design of an rfid-based battery-free programmable sensing platform," *IEEE Transactions on Instrumentation and Measurement*, vol. 57, no. 11, pp. 2608–2615, November 2008.

[4] Cavity resonator microphone (also known as the great seal bug). [Online]. Available: http://www.spybusters.com/Great_Seal_Bug.html

[5] R. Fletcher, J. A. Levitan, and J. Rosenberg, "Application of smart materials to wireless id tags and remote sensors," in *In Materials for Smart Systems II, Materials Research Society*, 1997, pp. 557–562.

[6] S. Johan, X. Zeng, T. Unander, A. Koptyug, and H.-E. Nilsson, "Remote moisture sensing utilizing ordinary rfid tags," in *Sensors, 2007 IEEE*, oct. 2007, pp. 308 –311.

[7] R. Bhattacharyya, C. Floerkemeier, and S. Sarma, "Low-cost, ubiquitous rfid-tag-antenna-based sensing," *Proceedings of the IEEE*, vol. 98, no. 9, pp. 1593 –1600, sept. 2010.

[8] V. Talla, M. Buettner, D. Wetherall, and J. Smith, "Hybrid analog-digital backscatter platform for high data rate, battery-free sensing," in *Wireless Sensors and Sensor Networks (WiSNet), 2013 IEEE Topical Conference on*, 2013.

[9] S. Best and B. Kaanta, "A tutorial on the receiving and scattering properties of antennas," *Antennas and Propagation Magazine, IEEE*, vol. 51, no. 5, pp. 26 –37, oct. 2009.

[10] P. Nikitin, K. Rao, and R. Martinez, "Differential rcs of rfid tag," *Electronics Letters*, vol. 43, no. 8, pp. 431 –432, 12 2007.

[11] R. Sarpeshkar, "Analog versus digital: Extrapolating from electronics to neurobiology," *Neural computation*, vol. 10, no. 7, pp. 1601–1638, October 1988.

[12] R. Walden, "Analog-to-digital converter survey and analysis," *Selected Areas in Communications, IEEE Journal on*, vol. 17, no. 4, pp. 539 –550, apr 1999.

[13] J. Koomey, S. Berard, M. Sanchez, and H. Wong, "Implications of historical trends in the electrical efficiency of computing," *Annals of the History of Computing, IEEE*, vol. 33, no. 3, pp. 46 –54, march 2011.

[14] S. Mandal, L. Turicchia, and R. Sarpeshkar, "A battery-free tag for wireless monitoring of heart sounds," in *Wearable and Implantable Body Sensor Networks, 2009. BSN 2009. Sixth International Workshop on*, june 2009, pp. 201 –206.

[15] M. Buettner and D. Wetherall, "A software radio-based uhf rfid reader for phy/mac experimentation," in *RFID (RFID), 2011 IEEE International Conference on*. IEEE, 2011, pp. 134–141.

[16] (2008) Tool for pesq analysis of speech. [Online]. Available: http://www.utdallas.edu/~loizou/speech/software.htm